



Frost, Ray L. and Soisnard, Aurore and Voyer, Nicolas and Palmer, Sara J. and Martens, Wayde N. (2009) *Thermo-Raman spectroscopy of selected layered double hydroxides of formula  $Cu_6Al_2(OH)_{16}CO_3$  and  $Zn_6Al_2(OH)_{16}CO_3$* . Journal of Raman Spectroscopy, 40(6). pp. 645-649.

© Copyright 2009 John Wiley & Sons

**Thermo-Raman spectroscopy of selected layered double hydroxides of formula  $\text{Cu}_6\text{Al}_2(\text{OH})_{16}\text{CO}_3$  and  $\text{Zn}_6\text{Al}_2(\text{OH})_{16}\text{CO}_3$**

**Ray L. Frost<sup>1,\*</sup>, Aurore Soisnard,<sup>1,2</sup> Nicolas Voyer<sup>1,2</sup>, Sara J. Palmer<sup>1</sup>, and Wayde N. Martens<sup>1</sup>**

*1 Inorganic Materials Research Program, School of Physical and Chemical Sciences, Queensland University of Technology, 2 George Street, Brisbane, GPO Box 2434, Queensland 4001, Australia.*

*2 ENSICEN, Ecole Nationale Supérieure d'Ingenieurs et Centre de Recherche, 6 Boulevard Marechal Juin 14050 Caen Cedex*

**Raman spectroscopy using a hot stage has been used to characterise layered double hydroxides (LDHs) of formula  $(\text{Cu,Zn})_6\text{Al}_2(\text{OH})_{16}(\text{CO}_3)\cdot 4\text{H}_2\text{O}$ . The spectra have been used to assess the molecular assembly of the cations in the LDH structure. The sharp band at  $1058\text{ cm}^{-1}$  for the  $\text{Zn}_6\text{Al}_2(\text{OH})_{16}(\text{CO}_3)\cdot 4\text{H}_2\text{O}$  is assigned to the  $\nu_1\text{ CO}_3^{2-}$  symmetric stretching mode. The band shifts to higher wavenumbers and is observed at  $1103\text{ cm}^{-1}$  at  $600^\circ\text{C}$ . It is proposed that metal carbonate species formed during the decomposition of the hydrotalcite structure is responsible for the increase in band position. The Cu-Al hydrotalcite did not show the same trend. The symmetric stretching mode of carbonate is observed at around  $1110\text{ cm}^{-1}$ , and at temperatures above  $200^\circ\text{C}$  a shoulder appears at around  $1210\text{ cm}^{-1}$ , suggested to be due to  $\text{CuCO}_3$ .**

**KEYWORDS:** dehydration, dehydroxylation, hydrotalcite, layered double hydroxide, hot stage Raman spectroscopy, infrared spectroscopy

---

\* Author to whom correspondence should be addressed (r.frost@qut.edu.au)

## INTRODUCTION

Hydrotalcites are natural minerals based upon a brucite structure in which the divalent cation ( $\text{Mg}^{2+}$ ) is replaced with a trivalent cation such as  $\text{Al}^{3+}$ , resulting in a positive charge on the brucite-like surface<sup>1-3</sup>. Hydrotalcite-like compounds, which are also known as layered double hydroxides, are anionic clays that are composed of positively charged hydroxyl layers  $[\text{M}^{\text{II}}_{1-x}\text{M}^{\text{III}}_x(\text{OH})_2]^{x+}$ , with interlayers containing anions, most commonly the carbonate anion, and water to provide overall charge neutrality. Many LDH type compounds can be synthesised in the laboratory. Hydrotalcites are given the general formula  $[\text{M}^{2+}_{(1-x)}\text{M}^{3+}_x(\text{OH})_2]^{x+}[\text{A}^{n-}]_{x/n}\cdot y\text{H}_2\text{O}$ , where  $\text{M}^{2+}$  and  $\text{M}^{3+}$  are the di- and trivalent cations in the octahedral positions within the hydroxide layers with  $x$  normally between 0.17 and 0.33<sup>4-6</sup>.  $\text{A}^{n-}$  is an exchangeable interlayer anion, which can be either organic or inorganic and indeed in practice is often a mixture of anions. An important property of hydrotalcites is its ability to exchange anions for others in the interlayers of the hydrotalcite. A large variety of anions can be incorporated into the interlayer region of LDHs using a range of methods: (1) anion-exchange, (2) co-precipitation, (3) rehydration of a calcined LDH, and (4) thermal activation reaction. This investigation utilised the co-precipitation method. Hydrotalcites intercalated with other anions such as phosphate, molybdate, vanadate have been synthesised<sup>7-9</sup>.

The synthesis of LDHs with anions other than carbonate must be carefully prepared to avoid contamination. The carbonate anion is readily incorporated and tenaciously held in the interlayer, and therefore creates problems when LDHs are synthesised to produce carbonate free LDHs. This can be overcome using a sealed system operating under a nitrogen atmosphere. Any water used in the synthesis of the hydrotalcites also needs to be boiled prior to use. The high affinity of the carbonate anion has been a main factor for it being a major counter anion for hydrotalcite. The abundant concentrations of carbon dioxide ( $\text{CO}_2$ ) present in the atmosphere can contribute to carbonate concentrations present in solutions.

Anion affinity for the LDH interlayer has been found to be based on the size of the ion and its associated charge. Monovalent anions have lower affinities than divalent anions and are therefore more likely to precipitate in anion exchange

reactions. The ease of exchange of monovalent anions is in the order  $\text{OH}^- > \text{F}^- > \text{Cl}^- > \text{Br}^- > \text{NO}_3^-$ <sup>10</sup>. Divalent anions such as  $\text{SO}_4^{2-}$  and  $\text{CO}_3^{2-}$  have higher selectivity than monovalent anions. Therefore, the most suitable LDH for anion-exchange syntheses are those that have monovalent anions in the interlayer due to the relative ease of exchange. The study of minerals, including hydrotalcites, by Raman spectroscopy has proven to be very useful<sup>11-21</sup>. Indeed Raman spectroscopy has proven most useful for the study of diagenetically related minerals as often occurs with hydrotalcite minerals<sup>22-28</sup>. Some previous studies have been undertaken by the authors using Raman spectroscopy to study hydrotalcites<sup>29-32</sup>. Spectroscopic studies, especially Raman studies, of hydrotalcites are limited especially where large anions are involved. The aim of this paper is to present Raman and infrared spectra of designed hydrotalcites with formula  $\text{Cu}_6\text{Al}_2(\text{OH})_{16}\text{CO}_3$  and  $\text{Zn}_6\text{Al}_2(\text{OH})_{16}\text{CO}_3$ .

## **EXPERIMENTAL**

### **Synthesis of hydrotalcite minerals**

Hydrotalcites with a composition of  $\text{Cu}_6\text{Al}_2(\text{OH})_{16}\text{CO}_3$  and  $\text{Zn}_6\text{Al}_2(\text{OH})_{16}\text{CO}_3$  were synthesised by the co-precipitation method. Two solutions were prepared using boiled ultra pure water: Solution 1 contained 2M NaOH and 0.125M  $\text{Na}_2\text{CO}_3$  while solution 2 contained 0.75M  $\text{Cu}^{2+}$  ( $\text{Cu}(\text{NO}_3)_2 \cdot 2.5\text{H}_2\text{O}$ ) (or 0.75M  $\text{Zn}^{2+}$  ( $\text{Zn}(\text{NO}_3)_2 \cdot 6\text{H}_2\text{O}$ )) and 0.25M  $\text{Al}^{3+}$  ( $\text{Al}(\text{NO}_3)_3 \cdot 6\text{H}_2\text{O}$ ). Solution 2 in the appropriate ratio was added to the solution 1 using a peristaltic pump at a rate of 25  $\text{cm}^3/\text{min}$ , under vigorous stirring. The precipitated minerals were vacuum filtration at ambient temperature and washed thoroughly with 0.1M  $\text{Na}_2\text{CO}_3$  solution to remove any residual nitrate salts. The hydrotalcites were centrifuged for 10 min and then washed again with boiled ultra pure water. The synthesised hydrotalcites were characterised using EDX analysis (elemental composition), X-Ray diffraction (crystal structure), and infrared and Raman Spectroscopy.

### **X-ray diffraction**

X-Ray diffraction patterns were collected using a Philips X'pert wide angle X-Ray diffractometer, operating in step scan mode, with Co  $\text{K}\alpha$  radiation (1.78897 Å).

Patterns were collected in the range  $3$  to  $75^\circ 2\theta$  with a step size of  $0.02^\circ$  and a rate of  $30$ s per step. Samples were in crushed powdered form.

### **Raman microscopy**

The crystals of hydrotalcite were placed on the stage of an Olympus BHSM microscope, equipped with  $10\times$  and  $50\times$  objectives and part of a Renishaw 1000 Raman microscope system, which also includes monochromators, a filter system and a Charge Coupled Device (CCD). Raman spectra were excited by a HeNe laser ( $633$  nm) at a nominal resolution of  $2$   $\text{cm}^{-1}$  in the range between  $100$  and  $4000$   $\text{cm}^{-1}$ . Details of the experimental technique have been published <sup>22-26,28,33-35</sup>.

### **Infrared Spectroscopy**

Infrared spectra were obtained using a Nicolet Nexus 870 FTIR spectrometer with a smart endurance single bounce diamond ATR cell. Spectra over the  $4000$ - $525$   $\text{cm}^{-1}$  range were obtained by the co-addition of  $128$  scans with a resolution of  $4$   $\text{cm}^{-1}$  and a mirror velocity of  $0.6329$   $\text{cm/s}$ .

Spectral Manipulation such as baseline adjustments, smoothing and normalisation was undertaken using the GRAMS® software package (Galactic Industries Corporation, Salem, NH, USA). Band component analysis was undertaken using the Jandel 'Peakfit' software package, which enabled the type of fitting function to be selected and allows specific parameters to be fixed or varied accordingly. Band fitting was done using a Lorentz- Gauss cross-product function with the minimum number of component bands used for the fitting process. The Lorentz- Gauss ratio was maintained at values greater than  $0.7$  and fitting was undertaken until reproducible results were obtained with squared correlations of  $r^2$  greater than  $0.995$ .

## **RESULTS AND DISCUSSION**

The unperturbed carbonate ion is a planar triangle with point symmetry  $D_{3h}$ . The free ion,  $\text{CO}_3^{2-}$  with  $D_{3h}$  symmetry exhibits four normal vibrational modes: (i) a symmetric stretching vibration ( $\nu_1$ ), (ii) an out-of-plane bend ( $\nu_2$ ), (iii) a doubly degenerate asymmetric stretch ( $\nu_3$ ), and (iv) a doubly degenerate bending mode ( $\nu_4$ ). The symmetries of these modes are  $A_1'$  (R) +  $A_2''$  (IR) +  $E'$  (R, IR) +  $E''$  (R, IR) and occur at 1063, 879, 1415 and 680  $\text{cm}^{-1}$ , respectively. Generally, strong Raman modes appear at around 1100  $\text{cm}^{-1}$  due to the symmetric stretching vibration ( $\nu_1$ ), of the carbonate groups, while intense IR and weak Raman peaks near 1400  $\text{cm}^{-1}$  are due to the antisymmetric stretch ( $\nu_3$ ). Infrared modes near 800  $\text{cm}^{-1}$  are derived from the out-of-plane bend ( $\nu_2$ ). Infrared and Raman modes around 700  $\text{cm}^{-1}$  region are due to the in-plane bending mode ( $\nu_4$ ). This mode is doubly degenerate for undistorted  $\text{CO}_3^{2-}$  groups. As the carbonate groups become distorted from regular planar symmetry, this mode splits into two components. Infrared and Raman spectroscopy provide a sensitive test for structural distortion of  $\text{CO}_3^{2-}$ . For the unperturbed carbonate anion the  $\nu_1$  mode is Raman active only. For the perturbed carbonate anion, all modes are both Raman and infrared active except for the  $\nu_2$  mode, which is IR active only.

The Raman spectra of the Zn-Al hydrotalcite in the 700 to 1700  $\text{cm}^{-1}$  region as a function of temperature is shown in Fig. 1. The sharp band at 1058  $\text{cm}^{-1}$ , at 100 °C, is assigned to the  $\nu_1$   $\text{CO}_3^{2-}$  symmetric stretching mode. The band shifts to higher wavenumbers as the temperature increases, with the  $\nu_1$   $\text{CO}_3^{2-}$  band shifting to 1103  $\text{cm}^{-1}$  at 600°C. Fig. 2 shows the variation of band centre of this vibrational mode as a function of temperature. The shift to higher wavenumbers is understood to be due to carbonate anions being in a different structural environment. Thermal analysis of the hydrotalcite structure showed that the dehydroxylation of the structure resulted in the formation of metal carbonate species, such as  $\text{ZnCO}_3$ , at temperatures above 350 °C. The presence of a shoulder at 1140 and 1160  $\text{cm}^{-1}$ , when the hydrotalcite is heated to 400 and 600 °C, suggests that this new metal carbonate species forms. Therefore it is proposed that the shift in band position is due to carbonate in the newly formed  $\text{ZnCO}_3$  and not in the interlayer of the hydrotalcite structure. However the compound is in low concentration and could not be detected by XRD. Thermal analysis shows the carbonate anion decomposes above this temperature, therefore Raman spectra were not obtained above 600 °C. The Raman spectra of the

Cu-Al hydrotalcite in the 700 to 1700  $\text{cm}^{-1}$  region as a function of temperature is shown in Fig. 3. The Cu-Al hydrotalcite observed the  $\nu_1 \text{CO}_3^{2-}$  symmetric stretching mode at higher wavenumbers than the Zn-Al hydrotalcite with the antisymmetric band being centred at around 1110  $\text{cm}^{-1}$ . Unlike the Zn-Al hydrotalcite, no increase in wavenumber is observed for the Cu-Al hydrotalcite as the temperature increases. It is proposed that the  $\text{CO}_3^{2-}$  is more strongly bonded to the hydrotalcite surface in the Cu-Al hydrotalcite than the Zn-Al hydrotalcite. The Cu-Al hydrotalcite shows greater stability and is not as easy as the Zn-Al hydrotalcite to decompose. The presence of a shoulder at around 1210  $\text{cm}^{-1}$  is attributed to the formation of  $\text{CuCO}_3$  as the hydrotalcite undergoes dehydroxylation at temperatures around 200  $^\circ\text{C}$ , observed by thermal analysis (Fig. not shown). The conclusion is reached that the carbonate anion is in two distinctly different environments in the hydrotalcite.

The weak broad band centred around 1590  $\text{cm}^{-1}$ , at 100  $^\circ\text{C}$ , for the Zn-Al hydrotalcite is proposed to be attributed to the HOH bending mode of non hydrogen bonded water. The intensity of the band increases significantly at 250  $^\circ\text{C}$ , and is believed to be  $\text{H}_2\text{O}$  trapped in the pores and vacant sites of the decomposing hydrotalcite structure. The intensity of the peak then decreases as the temperature rises to 400  $^\circ\text{C}$ , as at these temperatures water is removed from the structure as water vapour at these higher temperatures. No bands which are attributable to water are observed in the infrared spectrum. At 600  $^\circ\text{C}$  the band is absent, and it appears all  $\text{H}_2\text{O}$  has been removed from the hydrotalcite structure.

In the infrared spectra (Fig. 4) an intense infrared band at 1360  $\text{cm}^{-1}$  is attributed to the  $\nu_3$  antisymmetric stretching mode of carbonate. This band also shows some asymmetry on the high wavenumber side. The  $\text{CO}_3^{2-}$  symmetric stretching mode is very weak in the infrared spectrum. Low intensity bands are observed at 1095 and 1135  $\text{cm}^{-1}$  for the Zn-Al and Cu-Al hydrotalcites, respectively. A large broad band is observed for the Zn-Al hydrotalcite, centred at 770  $\text{cm}^{-1}$ , is attributed to the  $\nu_2$  out-of-plane bending mode of the carbonate anion. This band is not observed for the Cu-Al hydrotalcite, however, a less intense band is observed for Cu-Al hydrotalcite at 680  $\text{cm}^{-1}$  and is assigned to the in-plane bending mode.

The Raman spectrum of the Zn-Al and Cu-Al hydrotalcites in the low wavenumber region are shown in Figs 5 and 6, respectively. The Raman spectrum of brucite shows an intense band at  $442\text{ cm}^{-1}$ . The equivalent band in the hydrotalcite structure is around  $470\text{ cm}^{-1}$  depending on the degree of Zn substitution. This band is assigned to the MO symmetric stretching vibration. An intense band is observed at  $438\text{ cm}^{-1}$  for the Zn-Al hydrotalcite and is attributed to the ZnO stretching vibration. The intensity of this band increases with increasing temperature. Upon formation of the  $\text{Mg}_4\text{Zn}_2$  hydrotalcite two bands are observed in this region at  $481$  and  $467\text{ cm}^{-1}$ . For the  $\text{Mg}_2\text{Zn}_4$  hydrotalcite bands are observed at  $496$ ,  $481$  and  $466\text{ cm}^{-1}$ . The band is centred on  $491\text{ cm}^{-1}$  for the Zn-Al hydrotalcite. A band is also observed in brucite at  $367\text{ cm}^{-1}$ . Bands are observed at  $\sim 328$  and  $207\text{ cm}^{-1}$  for the Zn-Al hydrotalcite, and at  $297$  and  $219\text{ cm}^{-1}$  for the Cu-Al hydrotalcite. Upon thermal treatment the intensity of the bands at  $207$  and  $328\text{ cm}^{-1}$  decreases and approaches zero by  $600\text{ }^\circ\text{C}$ . It is proposed that these bands are associated with hydrogen bond formation between the OH units of the brucite-like layers and the interlayer anion. An intense band which is present at all temperatures is observed at  $148\text{ cm}^{-1}$  (Zn-Al hydrotalcite) and  $150\text{ cm}^{-1}$  (Cu-Al hydrotalcite) may be related to the OMO bending modes. Two overlapping bands are observed for the mixed divalent hydrotalcites.

## CONCLUSIONS

Insight into the unique structure and thermal stability of layered double hydroxides has been obtained using hot stage Raman spectroscopy. This research has tested the thermal stability of two synthesised hydrotalcites Zn-Al hydrotalcite and Cu-Al hydrotalcite. The importance of this work rests with the geosequestration of greenhouse gases. Thermally decomposed hydrotalcites may be used to soak up carbon dioxide from the atmosphere. Hydrotalcites have a ‘memory’ or reformation effect. If such minerals either natural or synthetic are used to react with greenhouse gases, it is important to know their structure and thermal stability.

The Raman band at  $1058\text{ cm}^{-1}$ , attributed to the symmetric stretching mode of carbonate, for the Zn-Al hydrotalcite observed a shift to higher wavenumbers,  $1103\text{ cm}^{-1}$ , at higher temperatures. It is proposed that the shift is due to the carbonate in a

different environment, and is believed to be carbonate in  $\text{ZnCO}_3$ , which forms during the dehydroxylation of the hydrotalcite structure. The same trend is not observed for the Cu-Al hydrotalcite, where the symmetric stretching mode of carbonate band remains centred around  $1110\text{ cm}^{-1}$  independent on temperature. It is proposed that the carbonate is more strongly bonded within the Cu-Al hydrotalcite structure. The band at around  $1210\text{ cm}^{-1}$  is believed to be due to the formation of  $\text{CuCO}_3$  that forms as the hydrotalcite structure undergoes dehydroxylation.

### **Acknowledgements**

The financial and infra-structure support of the Queensland Research and Development Centre (QRDC-Alcan) and the Queensland University of Technology Inorganic Materials Research Program of the School of Physical and Chemical Sciences is gratefully acknowledged.

## REFERENCES

1. Frost, RL, Ding, Z, Kloprogge, JT. *Can. J. Analyt. Sc. Spectrosc.* 2000.; **45**: 96.
2. Frost, RL, Ding, Z, Martens, WN, Johnson, TE, Kloprogge, JT. *Spectrochim. Act.* 2003; **59**: 321.
3. Hickey, L, Kloprogge, JT, Frost, RL. *J. Mater. Sci.* 2000; **35**: 4347.
4. Frost, RL, Erickson, KL. *J. Therm. Anal. Cal.* 2004; **76**: 217.
5. Kloprogge, JT, Wharton, D, Hickey, L, Frost, RL. *Am. Min.* 2002; **87**: 623.
6. Rives, V, Editor *Layered Double Hydroxides: Present and Future*, 2001.
7. Kloprogge, JT, Wharton, D, Hickey, L, Frost, RL. *Am. Min.* 2002; **87**: 623.
8. Smith, HD, Parkinson, GM, Hart, RD. *J. Cryst. Growth* 2005; **275**: e1665.
9. Smith, HD, Parkinson, GM. "Seawater Neutralisation: Factors affecting adsorption of anionic chemical species." 7th International Alumina Quality Workshop, 2005.
10. Newman, SP, Jones, W. *New J. Chem.* 1998; **22**: 105.
11. Frost, RL, Bouzaid, JM. *J. Raman Spectrosc.* 2007; **38**: 873.
12. Frost, RL, Bouzaid, JM, Martens, WN, Reddy, BJ. *J. Raman Spectrosc.* 2007; **38**: 135.
13. Frost, RL, Cejka, J. *J. Raman Spectrosc.* 2007; **38**: 1488.
14. Frost, RL, Cejka, J, Ayoko, GA, Weier, ML. *J. Raman Spectrosc.* 2007; **38**: 1311.
15. Frost, RL, Cejka, J, Weier, ML. *J. Raman Spectrosc.* 2007; **38**: 460.
16. Frost, RL, Cejka, J, Weier, ML, Martens, WN, Ayoko, GA. *J. Raman Spectrosc.* 2007; **38**: 398.
17. Frost, RL, Dickfos, MJ. *J. Raman Spectrosc.* 2007; **38**: 1516.
18. Frost, RL, Palmer, SJ, Bouzaid, JM, Reddy, BJ. *J. Raman Spectrosc.* 2007; **38**: 68.
19. Frost, RL, Pinto, C. *J. Raman Spectrosc.* 2007; **38**: 841.
20. Frost, RL, Weier, ML, Williams, PA, Leverett, P, Kloprogge, JT. *J. Raman Spectrosc.* 2007; **38**: 574.
21. Locke, AJ, Martens, WN, Frost, RL. *J. Raman Spectrosc.* 2007; **38**: 1429.
22. Frost, RL, Cejka, J, Ayoko, G. *J. Raman Spectrosc.* 2008; **39**: 495.
23. Frost, RL, Cejka, J, Ayoko, GA, Dickfos, MJ. *J. Raman Spectrosc.* 2008; **39**: 374.
24. Frost, RL, Dickfos, MJ, Cejka, J. *J. Raman Spectrosc.* 2008; **39**: 582.
25. Frost, RL, Hales, MC, Wain, DL. *J. Raman Spectrosc.* 2008; **39**: 108.
26. Frost, RL, Keeffe, EC. *J. Raman Spectrosc.* 2008; **in press**.
27. Frost, RL, Keeffe-, EC. *J. Raman Spectrosc.* 2008; **communicated**.
28. Palmer, SJ, Frost, RL, Ayoko, G, Nguyen, T. *J. Raman Spectrosc.* 2008; **39**: 395.
29. Frost, RL, Weier, ML, Kloprogge, JT. *J. Raman Spectrosc.* 2003; **34**: 760.
30. Kloprogge, JT, Hickey, L, Frost, RL. *J. Raman Spectrosc.* 2004; **35**: 967.
31. Frost, RL, Musumeci, AW, Martens, WN, Adebajo, MO, Bouzaid, J. *J. Raman Spectrosc.* 2005; **36**: 925.
32. Frost, RL, Musumeci, AW, Kloprogge, JT, Adebajo, MO, Martens, WN. *J. Raman Spectrosc.* 2006; **37**: 733.
33. Frost, RL, Cejka, J, Dickfos, MJ. *J. Raman Spectrosc.* 2008; **39**: 779.
34. Frost, RL, Locke, A, Martens, WN. *J. Raman Spectrosc.* 2008; **39**: 901.

35. Frost, RL, Reddy, BJ, Dickfos, MJ. *J. Raman Spectrosc.* 2008; **39**: 909.

**Fig. s**

Fig. 1: Raman spectrum of Zn-Al hydrotalcite in the carbonate vibrational region.

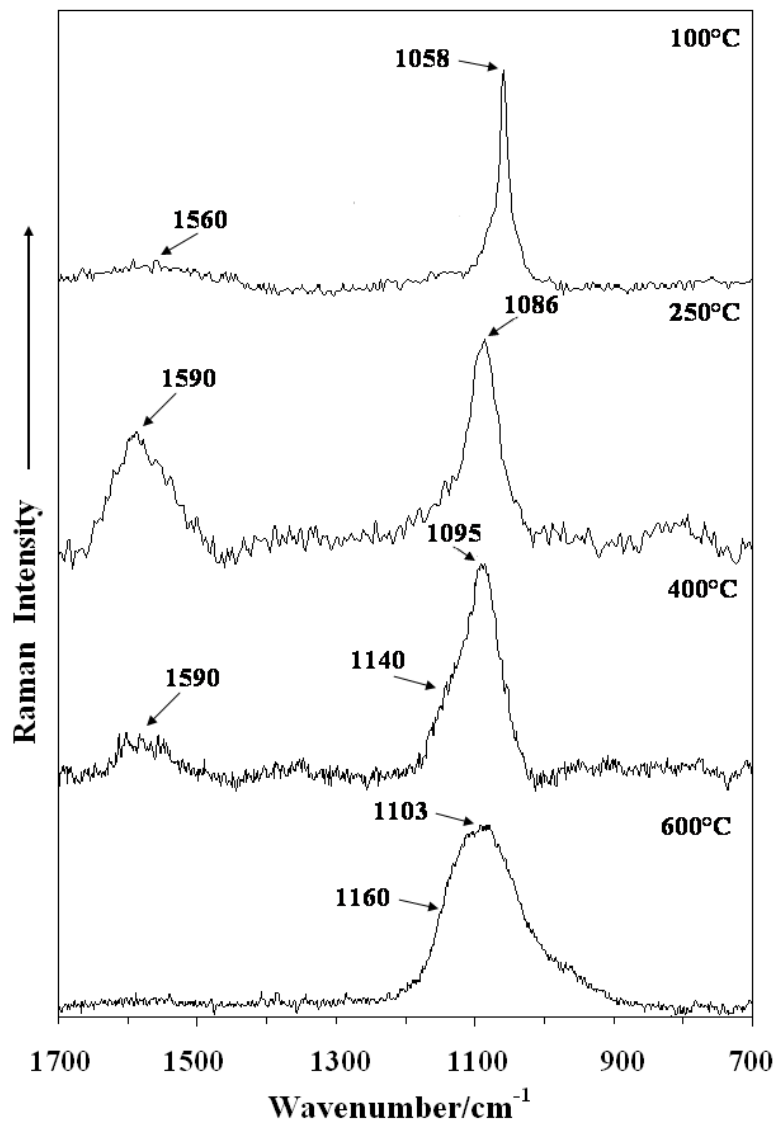
Fig. 2: Relationship between temperature and symmetric stretching mode of carbonate for the Zn-Al hydrotalcite around  $1100\text{ cm}^{-1}$ .

Fig. 3: Raman spectrum of Cu-Al hydrotalcite in the carbonate vibrational region.

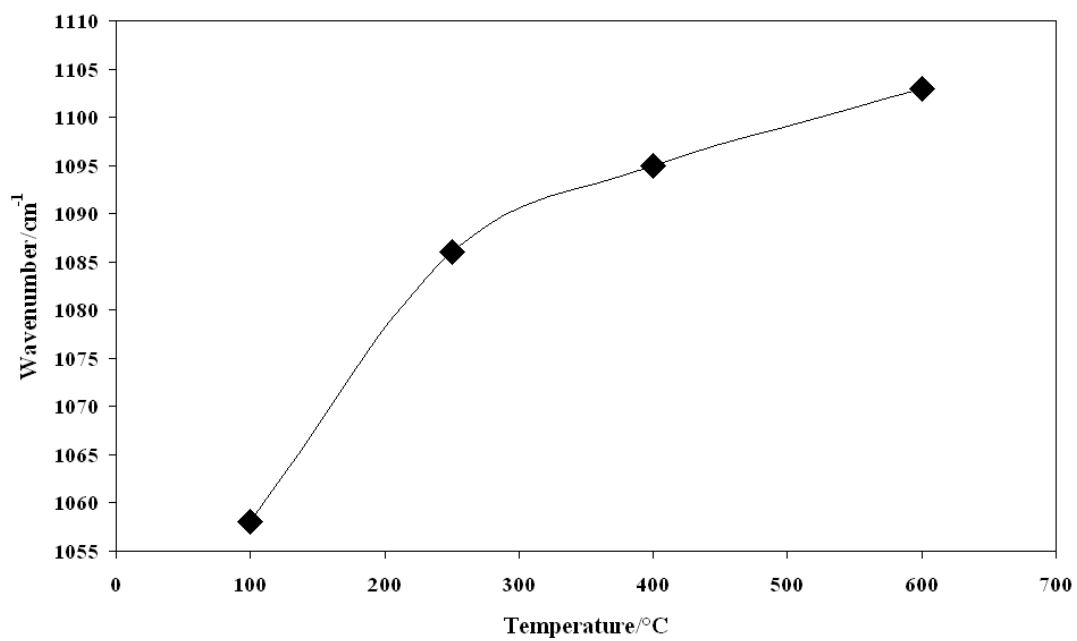
Fig. 4: Infrared spectra of Zn-Al and Cu-Al hydrotalcites.

Fig. 5: Raman spectra of Zn-Al hydrotalcite in the low wavenumber region.

Fig. 6: Raman spectra of Cu-Al hydrotalcite in the low wavenumber region.



**Fig. 1: Raman spectrum of Zn-Al hydroxalcite in the carbonate vibrational region.**



**Fig. 2: Relationship between temperature and symmetric stretching mode of carbonate for the Zn-Al hydrotalcite around 1100 cm<sup>-1</sup>.**

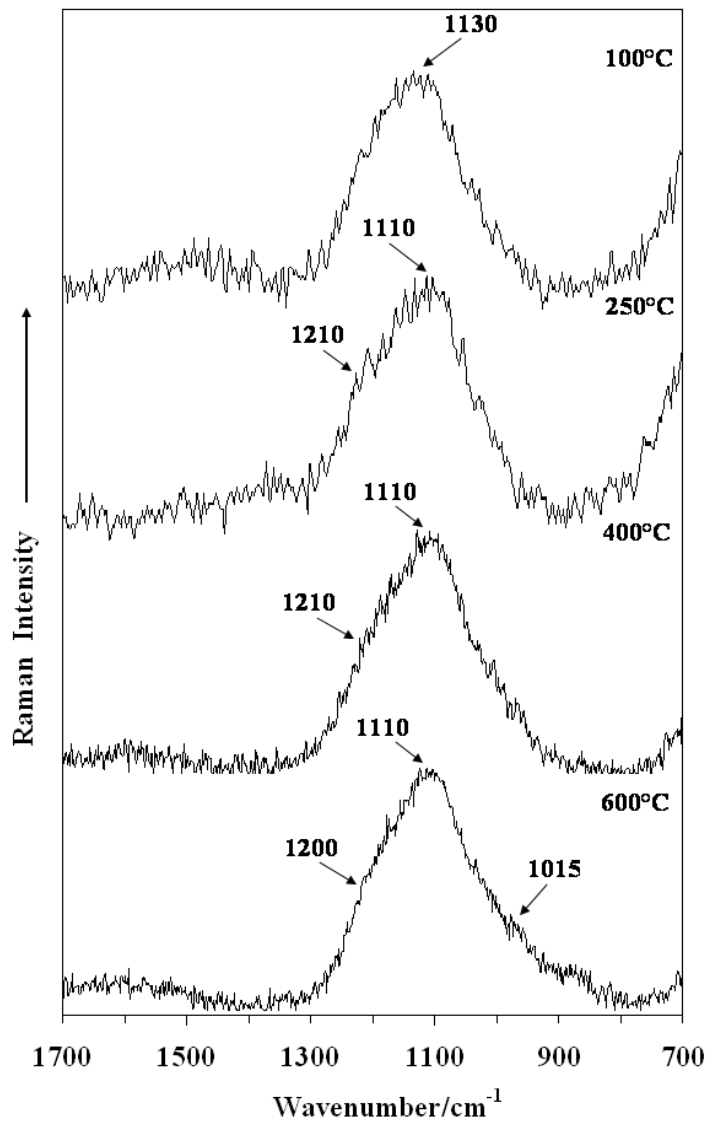


**Fig. 3: Raman spectrum of Cu-Al hydrotalcite in the carbonate vibrational region.**

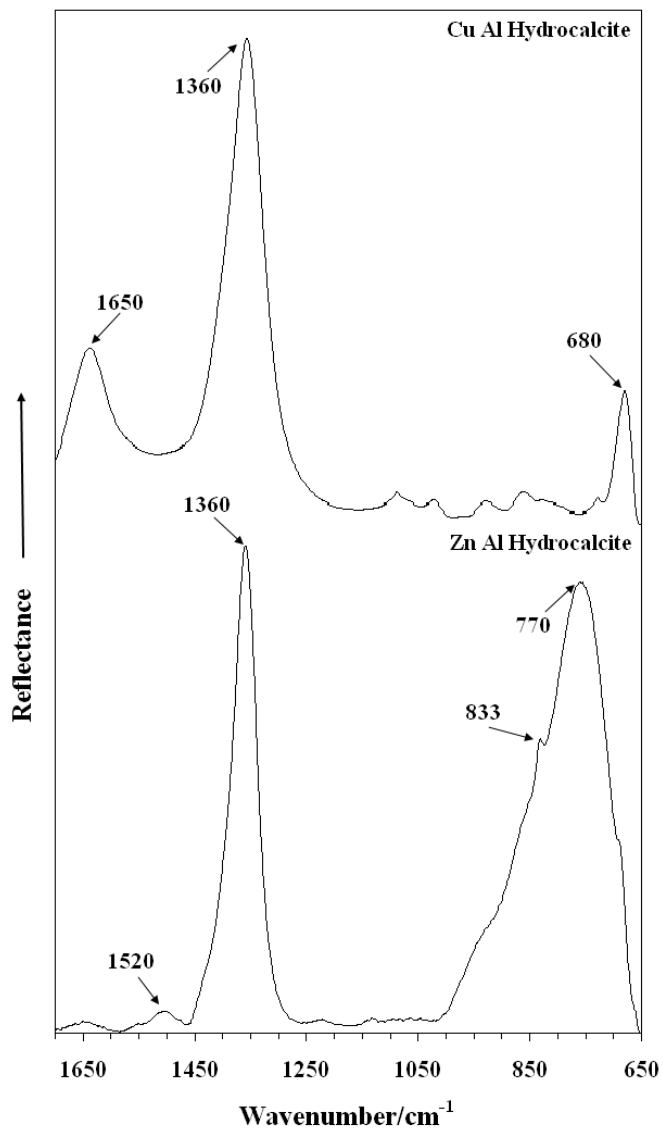


**Fig. 4: Infrared spectra of Zn-Al and Cu-Al hydroxaltes.**

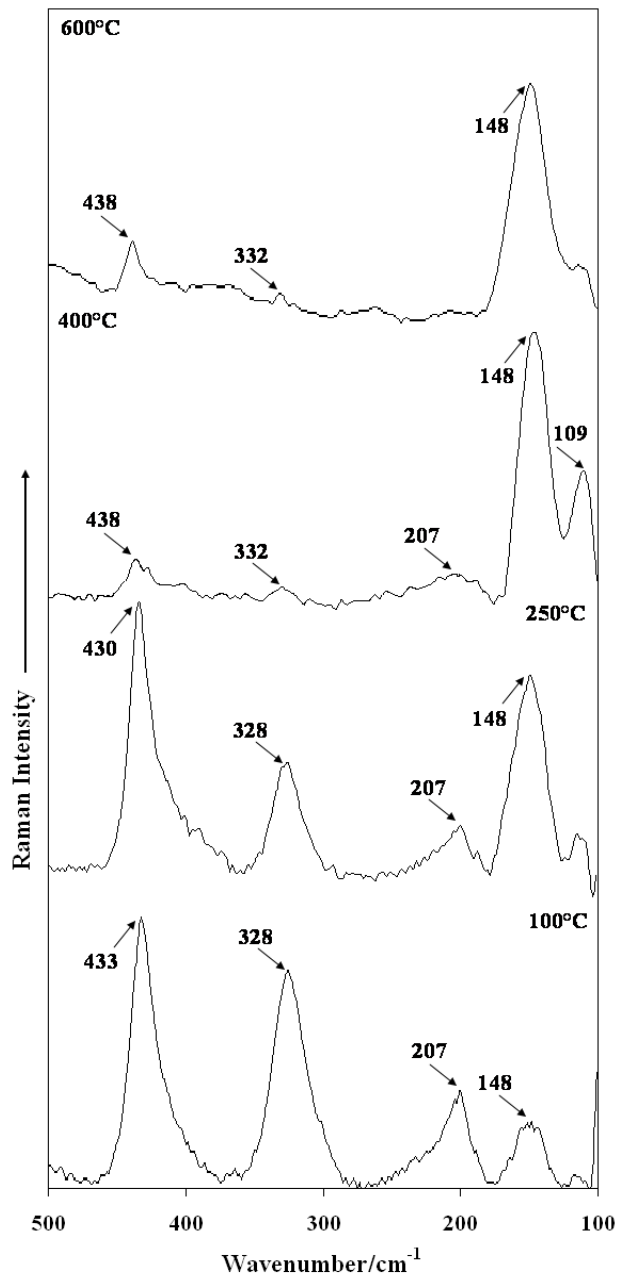


**Fig. 5: Raman spectra of Zn-Al hydrotalcite in the low wavenumber region.**

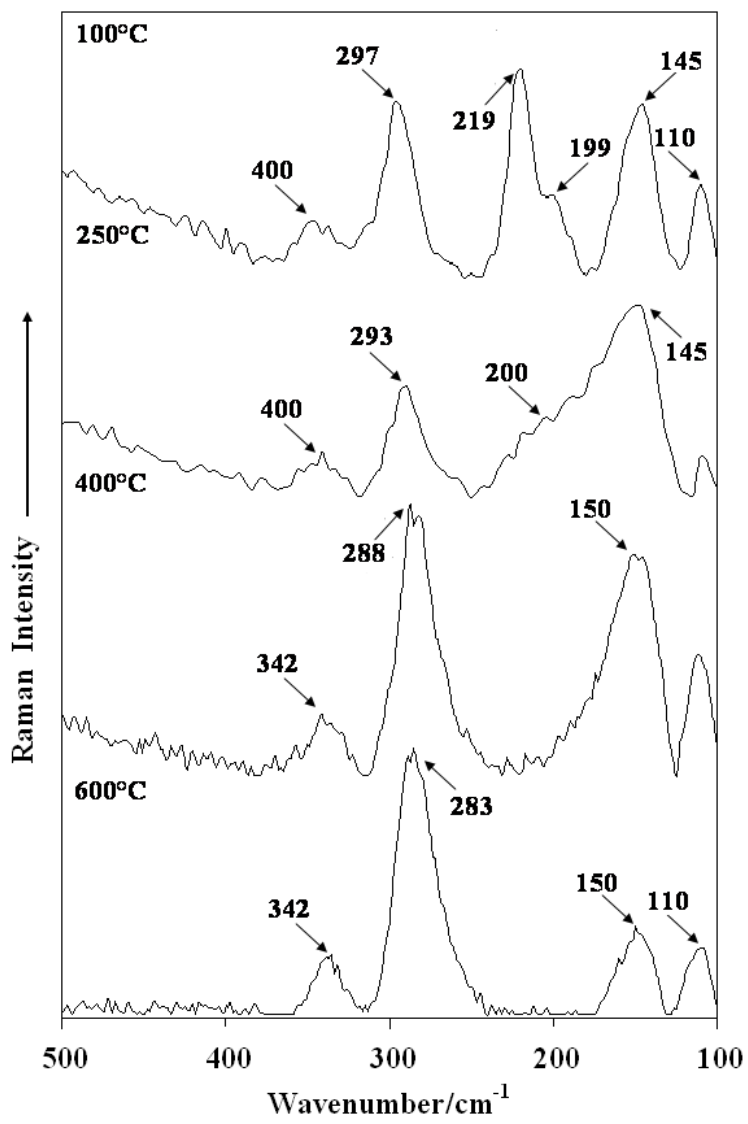


Fig. 6: Raman spectra of Cu-Al hydrotalcite in the low wavenumber region.